JACS
JOURNAL OF THE AMERICAN CHEMICAL SOCIETY
Communication
pubs.acs.org/JACS

Strategies to Design Efficient Silica-Supported Photocatalysts for Reduction of CO_2

Mohamed S. Hamdy,[†,‡] Rezvaneh Amrollahi,[†] Ilya Sinev,[§] Bastian Mei,[§] and Guido Mul*[,†]

[†]Photocatalytic Synthesis Group, Faculty of Science and Technology, MESA+ Institute for Nanotechnology, University of Twente, Enschede, The Netherlands

[‡]Chemistry Department, Faculty of Science, Helwan University, Cairo, Egypt

[§]Laboratory of Industrial Chemistry, Ruhr-University Bochum, 44780 Bochum, Germany

Supporting Information

ABSTRACT: The photocatalytic reduction of CO_2 by water vapor to produce light hydrocarbons was studied over a series of catalysts consisting of variable loading of Ti incorporated in TUD-1 mesoporous silica, either modified by ZnO nanoparticles or isolated Cr-sites. Unexpectedly, the performance of ZnO-Ti-TUD-1 and Cr-Ti-TUD-1 was inferior to the parent Ti-TUD-1. An explanation can be found in experiments on the photocatalytic degradation of a mixture of hydrocarbons (i.e., CH_4, C_2H_4, C_2H_6, C_3H_6, and C_3H_8) under the same illumination conditions. Ti-TUD-1 exhibits the poorest activity in hydrocarbon degradation, while ZnO-Ti-TUD-1 and Cr-Ti-TUD-1 showed very significant degradation rates. This study clearly demonstrates the importance of evaluating hydrocarbon conversion over photocatalysts active in converting CO_2 to hydrocarbons (in batch reactors).

Over the past decade, the contribution of solar panels to the production of electricity has significantly increased. To compensate for imbalances in energy production and demand and to sustain net stability, it is of eminent importance to create scalable solutions for storage of energy provided by sunlight. A possible route to store solar energy is to directly convert solar light into a fuel. Compared to hydrogen, (liquid) hydrocarbons have the advantage of an existing infrastructure, making production, distribution, and application of these environmentally benign solar fuels attractive. Prospective solar to fuel converters require the development of very efficient photocatalysts. Modifications of crystalline TiO_2-based catalysts have been reported extensively in the literature[1−6] to be active in light- and water-induced photocatalytic reduction of CO_2. In particular the effect of Cu-sites,[3] or attachment of metallic cocatalyst nanoparticles, such as Ag,[4] Pd,[5] or Pt,[6] has been evaluated. The currently best performing catalysts in direct CO_2 reduction to hydrocarbons, in particular on a per active site basis, are materials containing isolated Ti-sites in silica matrices, pioneered by Anpo and his co-workers in the 1990s.[7] Several silica matrices have been reported effective when hosting Ti-sites, including zeolites and mesoporous materials.[8−10] However, implementation of these materials in solar to fuel converters is still impractical, because of the low yields typically achieved with these catalysts.[11]

In this study, we evaluate three strategies to improve on the current standing of the intriguing catalysts on the basis of Ti-sites in silica matrices. First we adapt the pore structure and improve Ti dispersion by incorporation of Ti-sites in a TUD-1 silica matrix. Second we add ZnO to provide CO_2 adsorption capacity for times sunlight is not available for reaction,[12] and third we evaluate the performance of visible light sensitive Cr-O-Ti sites.[13] We provide novel insight in the synergy between TiO_x and ZnO nanoparticles as well as TiO_x, and CrO_x, not only regarding changes in the apparent CO_2 reduction rates but also in particular by discussing the ability and consequences of the newly created sites to convert hydrocarbons by water vapor and low concentrations of oxygen (coproduct of CO_2 reduction) to CO_2, according to reaction 1:

$$CxHy + H_2O + (O_2) \rightarrow [\text{intermediates}] \rightarrow CO_2 + H_2 + (H_2O) \quad (1)$$

The elemental analysis and textural properties of the samples prepared on the basis of the TUD-1 matrix, varying Ti-content and either having ZnO nanoparticles or Cr^{6+} centers as additional ingredients, are listed in Table S1. The composition of the catalysts reflects the synthesis gel compositions very well. The N_2 desorption/adsorption isotherms of the Ti-1, Ti1-Cr1, and Ti1-Zn10 samples (the numbers indicate the loading of the element in TUD-1) (Figure S1, left) are of type IV, representative for mesoporous materials according to IUPAC classification. The isotherm of the ZnO modified material (Zn-10) is slightly different as compared to the other composites, suggesting the formation of ZnO nanoparticles inside the pores. These ZnO nanoparticles are so small that they are not visible in XRD patterns. XRD patterns (Figure S1, right) only contain a broad diffraction line at around 23° which is indicative of well-ordered amorphous silica.[14]

UV−vis spectra of the prepared samples are plotted in Figure 1. All spectra were collected at ambient conditions. By comparison it is evident that the absorption band at 220 nm, assigned to isolated Ti sites in tetrahedral coordination,[15] is somewhat reduced in intensity in the presence of the ZnO nanoparticles, but generally the absorption features appear a composite of the individual contributions of the ZnO nanoparticles and the Ti sites. ZnO nanoparticles supported on silica usually show a broad adsorption band around 240−

Received: October 9, 2013
Published: December 18, 2013

dx.doi.org/10.1021/ja410363v | J. Am. Chem. Soc. 2014, 136, 594−597

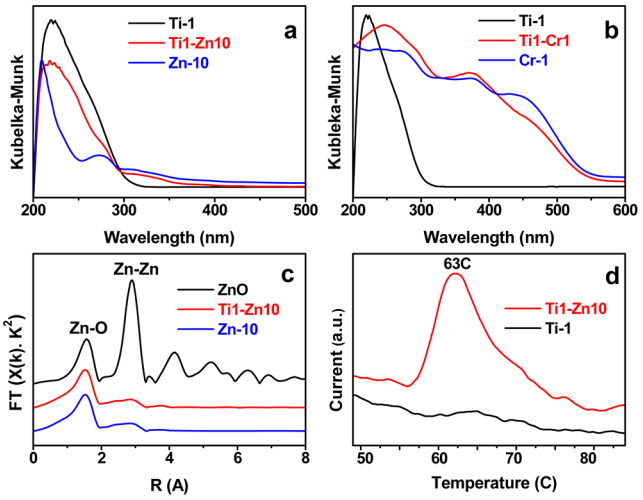

Figure 1. UV−vis DRS spectra of the modified Ti-TUD-1 catalysts recorded in ambient conditions: (a) the spectrum of the Ti-1-Zn-10 composite as compared to Zn-10 and Ti-1; (b) the spectrum of the Ti1-Cr1 sample as compared to Cr-1 and Ti-1; (c) ZnK EXAFS spectra of Zn-10 and Ti1-Zn10, compared to a reference ZnO sample; and (d) CO_2 TPD spectra of Ti-1 and Ti1-Zn10 samples.

400 nm.[16] We have also conducted analysis of the isolated Ti^{4+} content in samples Ti-1 to Ti-10 by reconstructing and comparing the DRS spectra in Figure S2. An estimate for the change in the amount of tetrahedral Ti^{4+} is included in Table S2. Isolated sites decrease in quantity from 99% to 58% when the Ti-loading increases from 1.0 to 10%. Further, we anticipate that a similar high amount of isolated centers (close to 100%) is present in the Ti-1, Ti1-Cr1, and Ti1-Zn10 catalysts.

Relative intensities in the spectrum of CrO_x sites appear very different when in the presence of Ti sites: the 480 nm absorption is reduced in intensity, whereas the relative intensity of the absorption at 375 nm increases. The 375 nm absorption and the shoulder at 480 nm are usually assigned to ligand to metal charge transfer (from O^{2-} to Cr^{6+}) of tetrahedrally coordinated Cr^{6+}.[17] Additionally, the absence of a peak around 600 nm is an indication that $Cr^{3+}O_x$ is not present in the samples.

In XANES spectra of the Ti1-Zn10 and Zn-10 samples (see Figure S3), the position of the ZnK X-ray absorption edge remains unchanged when in the presence of titanium, at ca. 9662.5 eV, which is 1 eV higher as compared to ZnO measured in the same conditions (9661.5 eV). We therefore conclude that zinc is present as Zn^{2+} in all samples. The spectral shape of the XANES postedge region of the two samples shows two relatively low maxima at 9664.6 and 9668.3 eV instead of one intense peak at 9668.7 eV typical for ZnO. This observation leads to the conclusion that a fraction of the Zn cations is located in the framework of TUD-1 as divalent cations and, more importantly, a considerable fraction of Zn is present in the form of ZnO nanoparticles. This is in agreement with the work of Yoshida et al.,[18] who attributed the small band at 9668 eV measured for ZnO/SiO_2 catalysts to formation of clusters/oligomers of tetrahedral $[ZnO_4]^{6-}$ units.

The EXAFS spectrum (in the Fourier transformation) of Ti1-Zn10 is compared to those of Zn-10 and ZnO in Figure 1c. Two distinct peaks are observed in the spectrum of ZnO. The first around 1.5 A is assigned to neighboring oxygen atoms in the first shell, while the second around 2.9 A is assigned to Zn atoms in the second shell. The similarity in spectra suggests that the zinc oxide species in the Zn-10 and Ti1-Zn10 samples have the same Zn-O bond length and coordination number as present in bulk ZnO (i.e., ZnO_4^{6-} tetrahedra). Furthermore, the spectra of Zn-10 and Ti1-Zn10 samples show a weak band around 2.5−3 A which is corresponding to the second shell (i.e., Zn-Zn). The weak intensity of this absorption indicates that the coordination number of neighboring Zn atoms would be very low, which is in agreement with the formation of nanoparticles of ZnO.[18] The presence of these nanoparticles is further confirmed in a micrograph of the Ti1-Zn10 sample (Figure S4). The characteristic morphology of TUD-1[19] and highly dispersed ZnO nanoparticles with a size of 5−7 nm, which is consistent with the pore diameter of this sample, [20] can be identified. To study the ability of the ZnO-containing samples to adsorb CO_2, temperature programmed desorption (TPD) of CO_2 adsorbed at room temperature was carried out (Figure 1d). A desorption peak of CO_2 at 63 °C was observed, which is absent in the curve of the Ti-1 sample. This confirms the ability of ZnO to bind CO_2 at room temperature which is easily released at slightly elevated temperatures. We have also analyzed the sorption of CO_2 on the ZnO sites by infrared spectroscopy (Figure S5) and compared this to CO_2 sorption on the Ti1-Cr1 catalyst. While features of adsorbed CO_2 can be clearly resolved in the IR spectra of Ti1-Zn10, suggesting formation of (bi)carbonates, these features are absent when the Ti1-Cr1 catalyst is exposed to CO_2. Clearly, the interaction of CO_2 with Cr sites is much weaker than with the ZnO nanoparticles.

Before discussion of the photocatalytic performance of the samples, it is important to note that removal of hydrocarbon residue, present in the samples as a consequence of the preparation procedure, is essential to confirm conversion of CO_2. Even after calcination at elevated temperature, small amounts of methane are typically observed upon illumination of the catalysts in the presence of water vapor.[21] Therefore, five cycles of treatment in humidified He were used to remove residual carbon, typically apparent by formation of methane. First we will discuss the effect of the Ti loading on the hydrocarbon formation efficacy, presented in Figure 2a. Two

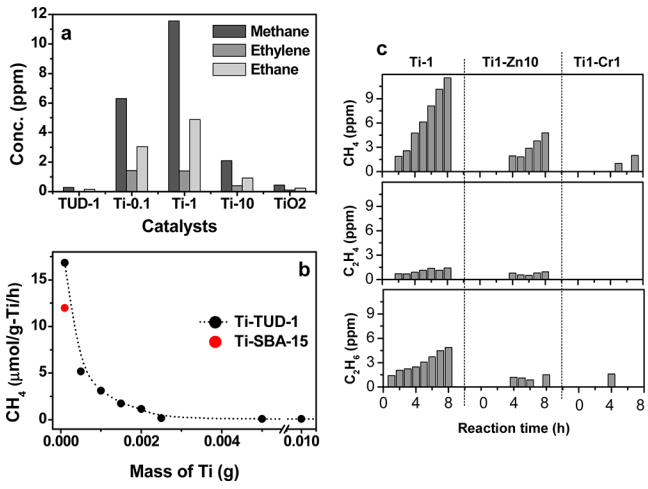

Figure 2. Concentrations of (a) hydrocarbons (i.e., methane, ethylene and ethane) produced after 8 h of illumination over different Ti-TUD-1 samples and Hombikat TiO_2 and (b) methane per mass of titanium for the different Ti-TUD-1 samples and Ti-SBA-15. (c) A comparison between the concentrations of produced hydrocarbons over Ti-1, Ti1-Zn10, and Ti1-Cr1, as a function of time.

dx.doi.org/10.1021/ja410363v | J. Am. Chem. Soc. 2014, 136, 594−597

reference samples, siliceous TUD-1 and TiO_2 Hombikat (the latter consisting of a high surface area anatase phase), show minor quantities of products. Of the Ti-TUD-1 samples, Ti-1 is the most active, showing methane, ethylene, and ethane as products. The amount of produced hydrocarbons is higher than obtained using Ti-0.1 or Ti-10. This can be explained by the amount of isolated tetrahedrally coordinated Ti^{4+} species available for the reaction. This increases comparing Ti-0.1 and Ti-1 and decreases comparing Ti-1 and Ti-10 (Table S2). Ti-10 contains nanoparticles of TiO_2 (octahedrally coordinated Ti-sites) inside the pores of TUD-1,[20] which are less effective in apparent hydrocarbon formation.[7]

Figure 2b shows the decreasing trend in methane production rate as a function of increasing Ti-mass, confirming isolated Ti^{4+} centers provide the optimal catalytic environment for hydrocarbon production. A comparison between the photocatalytic rates of Ti-TUD-1 and Ti-SBA-15 showed a 30% increase in the total hydrocarbons produced for TUD-1. The advantage of using TUD-1 as a support lies in the relatively high Ti loading that can be applied, before loss of dispersion of isolated tetrahedrally coordinated sites is apparent. Improved dispersion of Ti-sites in TUD-1 as compared to other mesoporous materials has been reported previously.[22] The Ti-1 sample is catalytically stable: Figure S6 shows reproducibility in the amount of products formed, when using the Ti-1 sample in 6 consecutive runs.

The photocatalytic performance of the Ti-1 sample is compared to the performance of Ti1-Zn10 and Ti1-Cr1 in Figure 2c. Surprisingly, the performance of Ti-1 is significantly better than of the modified samples. Ti-1 showed less than half in productivity after incorporation of the ZnO nanoparticles. The detrimental effect of adding Cr is even worse: Ti-1 almost completely lost its efficacy.

An explanation for the adverse effect of the modifications of the catalyst can be found in the following experiments. A mixture of five different hydrocarbons CH_4, C_2H_4, C_2H_6, C_3H_6, and C_3H_8 was exposed to the catalyst formulations in the presence of light and water vapor, and the result is shown in Figure 3. Not surprisingly, methane only slowly degrades over the catalytic systems in a period of 120 min of illumination. The saturated hydrocarbons (i.e., ethane and propane) are less stable than methane, and significant conversion can be observed, in particular over the Ti-1-Cr-1 sample. Depending on catalyst composition, unsaturated hydrocarbons (i.e., ethylene and propylene) were degraded very efficiently. An order in photocatalytic performance of Ti1-Cr1 > Zn-10 > Cr-1 > Ti1-Zn10 > Ti-1 has been identified. This experiment shows how important evaluation of the back-reaction of hydrocarbons is in explaining performance of catalysts in CO_2 reduction, in particular if batch reactors are used. This is often necessary to reach concentrations of products detectable by flame ionization detectors of GC equipment. It should also be noted that the activity of Ti-10 and in particular Hombikat TiO_2 is significantly higher in hydrocarbon oxidation, as compared to Ti-1 (Figure S7), which might explain the usually observed poor performance of, e.g., modified crystalline TiO_2 in CO_2 reduction.

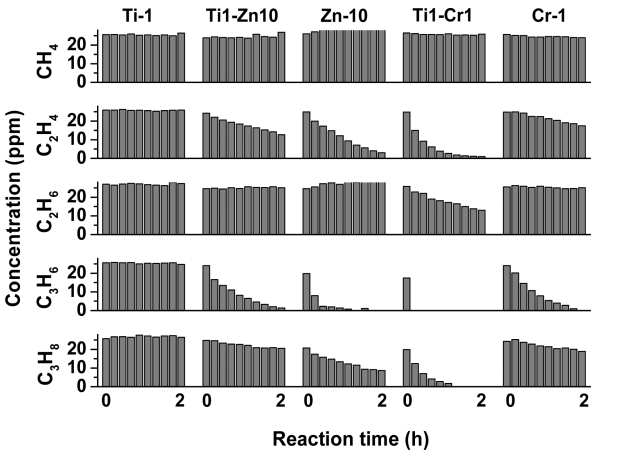

Figure 3. Degradation profiles of the standard hydrocarbons over the prepared samples. The concentrations were recorded every 15 min for the duration of 2 h.

To the best of our knowledge, the absence of photocatalyic oxidation activity of methane and ethane over purely tetrahedrally coordinated Ti supported on silica has not been reported previously. However, the extent of activity of the catalysts active in hydrocarbon oxidation is generally in agreement with literature observations. Yamashita et al.[23] showed that whereas ethylene was hardly activated by Ti-MCM-41, propylene[24] and propane[20,25] are significantly converted. It has also been reported that methane, ethane, and propane can be oxidized over ZnO-containing catalysts at slightly elevated temperatures, T = 493 K (Wada et al.)[26] and 500−550 K (Watanabe et al.).[27] We show photocatalytic conversion of propane is also feasible over silica supported nanoparticles of ZnO at room temperature. $Cr^{6+}O_x$ supported on silica was found to activate propane[28] and propylene.[29] Moreover, the synergy between Ti^{4+} and Cr^{6+} for hydrocarbon degradation observed in Figure 3 is in agreement with the pioneering work of Yamashita et al., who observed activation of propane using Cr-Ti-MCM-41,[23] Cr-Ti-HMS, and Cr-Ti-zeolites,[30] respectively.

The small conversion rate of methane shown in Figure 3 does not come in complete agreement with the significant reduction in formation of this product in the CO_2 reduction experiments shown in Figure 2c. We believe this is due to reverse, rather than forward, reactions of intermediates and in particular formaldehyde.[31] It has been reported that ZnO can photodegrade formaldehyde to carbon dioxide and water.[32] The degradation of formaldehyde to CO_2 likely also contributes to the negative effect of Cr^{6+} ions on performance of Ti-TUD-1 in production of methane. Cr^{6+} was reported to significantly enhance the performance of TiO_2 in the degradation of formaldehyde.[33] To demonstrate the conversion of formaldehyde, the Supporting Information contains *in situ* diffuse reflectance infrared spectra of light-induced conversion of formaldehyde in the presence of water vapor (Figure S8). Comparing the spectra of Ti-1 to that of Ti1-Cr1, the Cr-containing sample displays the signature of vibrational modes of formates, which are completely absent in the spectrum of the Ti-1 catalyst. Bands at 1580, ~1370, and 1350 cm^{-1} can be assigned to the ν_{as} OCO, δ C-H, and ν_s OCO modes of formates, respectively.[34] One last observation from the data of Figure 3 needs explanation: the Ti1-Zn10 sample exhibits an apparent photocatalytic degradation activity toward ethylene, propylene, and propane which is significantly smaller than of the Zn-10 catalyst. Presumably, CO_2 produced by conversion of hydrocarbons over the ZnO nanoparticles is converted reversibly to hydrocarbons over the Ti-centers, in agreement with the data of Figure 2c.

dx.doi.org/10.1021/ja410363v | *J. Am. Chem. Soc.* 2014, 136, 594−597

In summary, of the three modifications of silica supported Ti catalysts, alteration of the silica support has led to improvement in catalytic performance, explained by the relatively high loadings that can be achieved in TUD-1 without losing Ti-dispersion. Addition of ZnO nanoparticles leads to a smaller apparent rate in hydrocarbon production, despite the achieved storage capacity for CO_2. Adding visible light absorption functionality by CrO_x is even more detrimental to the observed production of hydrocarbons. Both ZnO and CrO_x addition to Ti-TUD-1 lead to significantly enhanced rates in the backward reactions of intermediates, such as formaldehyde, as well as of the produced hydrocarbons (in particular ethylene).

This study clearly demonstrates the importance of evaluating hydrocarbon oxidation over materials designed for CO_2 reduction. Photocatalyst and process development should attempt to minimize hydrocarbon conversion in process conditions needed for CO_2 reduction. Controlling water vapor pressure appears the challenge, since this is the main hydrocarbon oxidant and at the same time essential for the first step in activating CO_2.

■ ASSOCIATED CONTENT

Supporting Information

Experimental details and spectra data. This information is available free of charge via the Internet at http://pubs.acs.org.

■ AUTHOR INFORMATION

Corresponding Author

g.mul@utwente.nl

Notes

The authors declare no competing financial interest.

■ ACKNOWLEDGMENTS

The authors gratefully acknowledge Dr. Strunk and Prof. Dr. Muhler from the Ruhr-University Bochum for fruitful discussions.

■ REFERENCES

(1) Inoue, T.; Fujishima, A.; Koni, S.; Honda, K. *Nature* **1979**, *277*, 637.

(2) (a) Tan, S. S.; Zou, L.; Hu, E. *Catal. Today* **2006**, *115*, 269. (b) Mizuno, T.; Adachi, K.; Ohta, K.; Saji, A. *J. Photochem. Photobiol. A* **1996**, *98*, 87. (c) Kaneco, S.; Shimizu, Y.; Ohta, K.; Mizuno, T. *J. Photochem. Photobiol. A* **1998**, *115*, 223.

(3) Tseng, I. H.; Chang, W. C.; Wu, J. C. S. *Appl. Catal., B* **2002**, *37*, 37.

(4) Krejčíková, S.; Matějová, L.; Kočí, K.; Obalová, L.; Matěj, Z.; Čapek, L.; Šolcová, O. *Appl. Catal., B* **2012**, *111*−*112*, 119.

(5) Yui, T.; Kan, A.; Saitoh, C.; Koike, K.; Ibusuki, T.; Ishitani, O. *ACS Appl. Mater. Interfaces* **2011**, *3*, 2594.

(6) Pan, J.; Wu, X.; Wang, L.; Liu, G.; Lu, G. Q.; Cheng, H. M. *Chem. Commun.* **2011**, *47*, 8361.

(7) Anpo, M.; Chiba, K. *J. Mol. Catal.* **1992**, *74*, 207.

(8) Yamashita, H.; Fujii, Y.; Ichihashi, Y.; Zhang, S. G.; Ikeue, K.; Park, D. R.; Koyano, K.; Tatsumi, T.; Anpo, M. *Catal. Today* **1998**, *45*, 221.

(9) Ikeue, K.; Yamashita, H.; Anpo, M.; Takewaki, T. *J. Phys. Chem. B* **2001**, *105*, 8350.

(10) (a) Yang, H. C.; Lin, H. Y.; Chien, Y. S.; Wu, J. S.; Wu, H. H. *Catal. Lett.* **2009**, *131*, 381. (b) Yang, C. C.; Vernimmen, J.; Meynen, V.; Cool, P.; Mul, G. *J. Catal.* **2011**, *284*, 1.

(11) (a) Dhakshinamoorthy, A.; Navalon, S.; Corma, A.; Garcia, H. *Energy Environ. Sci.* **2012**, *5*, 9217. (b) Mori, K.; Yamashita, H.; Anpo, M. *RSC Adv.* **2012**, *2*, 3165.

(12) Mei, B.; Becerikli, A.; Pougin, A.; Heeskens, D.; Sinev, I.; Grunert, W.; Muhler, M.; Strunk, J. *J. Phys. Chem. C* **2012**, *116*, 14318.

(13) (a) Davydov, L.; Reddy, E. P.; France, P.; Smirniotis, P. G. *J. Catal.* **2001**, *203*, 157. (b) Shen, S.; Guo, L. *Catal. Today* **2007**, *129*, 414.

(14) (a) Adam, F.; Chew, T. S.; Andas, J. *J. Sol-Gel Sci. Technol.* **2011**, *59*, 580. (b) Chen, W.; Cai, W.; Zhang, L.; Wang, G.; Zhang, L. *J. Colloid Interface Sci.* **2001**, *238*, 291.

(15) Klein, S.; Weckhuysen, B. M.; Martens, J. A.; Maier, W. F.; Jacobs, P. A. *J. Catal.* **1996**, *163*, 489.

(16) (a) Tkachenko, O. P.; Klementiev, K. V.; Loffler, E.; Ritzkopf, I.; Schuth, F.; Bandyopadhyay, M.; Grabowski, S.; Gies, H.; Hagen, V.; Muhler, M.; Lu, L.; Fischer, R. A.; Grunert, W. *Phys. Chem. Chem. Phys.* **2003**, *5*, 4325. (b) Bahnemann, D. W.; Kormann, C.; Hoffmann, M. R. *J. Phys. Chem.* **1987**, *91*, 3789.

(17) (a) Zou, J. J.; Liu, Y.; Pan, L.; Wang, L.; Zhang, X. *Appl. Catal., B* **2010**, *95*, 439. (b) Zhang, L.; Zhao, Y.; Dai, H.; He, H.; Au, C. T. *Catal. Today* **2008**, *131*, 42.

(18) Yoshida, H.; Shimizu, T.; Murata, C.; Hattori, T. *J. Catal.* **2003**, *220*, 226.

(19) Jansen, J. C.; Shan, Z.; Marchese, L.; Zhou, W.; Puil, N. v. d.; Maschmeyer, T. *Chem. Commun.* **2001**, 713.

(20) Hamdy, M. S.; Berg, O.; Jansen, J. C.; Maschmeyer, T.; Moulijn, J. A.; Mul, G. *Chem.—Eur. J.* **2006**, *12*, 620.

(21) Yang, C. C.; Yu, Y. H.; van der Linden, B.; Wu, J. C. S.; Mul, G. *J. Am. Chem. Soc.* **2010**, *132*, 8398.

(22) (a) Wang, C. X. S.; Gaffney, A.; Song, R. In Proceedings of 245th ACS Meeting, New Orleans, LA, April 6-10, 2013; ACS: Washington, D.C., 2013. (b) Imran, G.; Pachamuthu, M.; Maheswari, R.; Ramanathan, A.; Sardhar Basha, S. J. *J. Porous Mater.* **2012**, *19*, 677. (c) Guo, Z.; Zhou, C.; Hu, S.; Chen, Y.; Jia, X.; Lau, R.; Yang, Y. *Appl. Catal., A* **2012**, *419*−*420*, 194. (d) Heikkilä, T.; Salonen, J.; Tuura, J.; Kumar, N.; Salmi, T.; Murzin, D. Y.; Hamdy, M. S.; Mul, G.; Laitinen, L.; Kaukonen, A. M.; Hirvonen, J.; Lehto, V.-P. *Drug Delivery* **2007**, *14*, 337.

(23) Kamegaw, T.; Shudo, T.; Yamashita, H. *Top. Catal.* **2010**, *53*, 555.

(24) (a) Yamashita, H.; Nishio, S.; Katayama, I.; Nishiyama, N.; Fujii, H. *Catal. Today* **2006**, *111*, 254. (b) Yoshida, H.; Murata, C.; Hattori, T. *J. Catal.* **2000**, *194*, 364.

(25) Hu, Y.; Wada, N.; Tsujimaru, K.; Anpo, M. *Catal. Today* **2007**, *120*, 139.

(26) Wada, K.; Yoshida, K.; Takatani, T.; Watanabe, Y. *Appl. Catal., A* **1993**, *99*, 21.

(27) Wada, K.; Yoshida, K.; Watanabe, Y.; Suzuki, T. *Chem. Commun.* **1991**, 726.

(28) Hamdy, M. S.; Berg, O.; Jansen, J. C.; Maschmeyer, T.; Arafat, A.; Moulijn, J. A.; Mul, G. *Catal. Today* **2006**, *117*, 337.

(29) Shi, X.; Ji, S.; Wang, K. *Catal. Lett.* **2008**, *125*, 331.

(30) (a) Masui, Y.; Ohshiro, S.; Anpo, M.; Ohmichi, T.; Katayama, I.; Yamashita, H. *e-J. Surf. Sci. Nanotechnol.* **2005**, *3*, 448. (b) Ohshiro, S.; Chiyoda, O.; Maekawa, K.; Masui, Y.; Anpo, M.; Yamashita, H. *C. R. Acad. Sci., Ser. IIc: Chim.* **2006**, *9*, 846.

(31) Mei, B.; Pougin, A.; Strunk, J. *J. Catal.* **2013**, *306*, 184.

(32) (a) Ai, Z.; Lee, S.; Huang, Y.; Ho, W.; Zhang, L. *J. Hazard Mater.* **2010**, *179*, 141. (b) Liao, Y.; Xie, C.; Liu, Y.; Huang, Q. *J. Alloys Compd.* **2013**, *550*, 190.

(33) (a) Lam, R. C. W.; Leung, M. K. H.; Leung, D. Y. C.; Vrijmoed, L. L. P.; Yam, W. C.; Ng, S. P. *Sol. Energy Mater. Sol. Cells* **2007**, *91*, 54. (b) Michalow, K. A.; Otal, E. H.; Burnat, D.; Fortunato, G.; Emerich, H.; Ferri, D.; Heel, A.; Graule, T. *Catal. Today* **2013**, *209*, 47.

(34) Kung, M. C.; Lin, S.-Y.; Kung, H. H. *Top. Catal.* **2012**, *55*, 108.